Design and performance of the prototype full field breast tomosynthesis system with selenium based flat panel detector

Baorui Ren [a], Chris Ruth [a], Jay Stein [a], Andrew Smith [a], Ian Shaw [b], Zhenxue Jing [c]
[a] Hologic, Inc., 35 Crosby Drive, Bedford, MA 01730
[b] Hologic / Lorad, 36 Apple Ridge Road, Danbury, CT 06810
[c] Hologic / Direct Radiography, 600 Technology Drive, Newark, DE 19702

ABSTRACT

We have developed a breast tomosynthesis system utilizing a selenium-based direct conversion flat panel detector. This prototype system is a modification of Selenia, Hologic's full field digital mammography system, using an add-on breast holding device to allow 3D tomosynthetic imaging. During a tomosynthesis scan, the breast is held stationary while the x-ray source and detector mounted on a c-arm rotate continuously around the breast over an angular range up to 30 degrees. The x-ray tube is pulsed to acquire 11 projections at desired c-arm angles. Images are reconstructed in planes parallel to the breastplate using a filtered backprojection algorithm. Processing time is typically 1 minute for a 50 mm thick breast at 0.1 mm in-plane pixel size, 1 mm slice-to-slice separation. Clinical studies are in progress.

Performance evaluations were carried out at the system and the subsystem levels including spatial resolution, signal-to-noise ratio, spectra optimization, imaging technique, and phantom and patient studies. Experimental results show that we have successfully built a tomosynthesis system with images showing less structure noise and revealing 3D information compared with the conventional mammogram. We introduce, for the first time, the definition of "Depth of Field" for tomosynthesis based on a spatial resolution study. This parameter is used together with Modulation Transfer Function (MTF) to evaluate 3D resolution of a tomosynthesis system as a function of system design, imaging technique, and reconstruction algorithm. Findings from the on-going clinical studies will help the design of the next generation tomosynthesis system offering improved performance.

Keywords: Breast tomosynthesis, full field digital mammography, flat panel detector, selenium direct conversion detector, MTF, depth of field, signal to noise ratio, spatial resolution, and spectra optimization.

INTRODUCTION

Breast cancer is the third leading cause of death among women in the U.S. and is the leading cause of death in women ages 40-55. Screening mammography, through early detection, has played a substantial role in reducing the mortality rate by 20% in the last decade. However invaluable mammography has been, its resultant efficacy is lowered by structure noise: tissue overlap that obscures lesions. Additionally, conventional mammography has limited efficacy in imaging denser breast tissues, often found in younger women, and postmenopausal women undergoing hormone replacement therapy.

Tomosynthesis, which is a 3-D digital mammography imaging technology, has shown significant early promise in addressing these imaging limitations. Tomosynthesis consists of taking x-ray images at multiple angles about a stationary compressed breast. The images are reconstructed into a 3-D dataset, which can be viewed in thin slices with high in-plane resolution that do not suffer from tissue overlap confusion. This can be achieved with only a modest increase in total examination time and at similar doses to conventional mammographic exams. Work has been reported on systems using this principle [1,2] and early clinical results have been encouraging [3-5].

We have developed a prototype breast tomosynthesis system using a selenium based direct conversion flat panel detector. In this paper, we will describe some basic information on the configuration and operation, performance analysis and characterization of this system. Results from both experiments and simulation studies will be given to cover various aspects of the performance of the system.

Medical Imaging 2005: Physics of Medical Imaging, edited by Michael J. Flynn,
Proceedings of SPIE Vol. 5745 (SPIE, Bellingham, WA, 2005)
1605-7422/05/$15 · doi: 10.1117/12.595833

DESCRIPTION OF THE OVERALL SYSTEM

The prototype breast tomosynthesis system was built by adding a removable breast holding device to the existing Selenia digital mammographic product, making it a dual modality unit. The Selenia gantry hosts a selenium based direct conversion flat panel detector and an x-ray tube on a c-arm system. The design allows the gantry to have two modes of operation. In the conventional mode, both the c-arm and the add-on breast holder can move together synchronously for an angular range of +/- 90 degrees. In the tomosynthesis mode, the add-on breast holder is kept stationary at any pre-set location within the above +/- 90 degrees range, such as for CC or MLO view shots, with the c-arm rotating independently of the breast holder. The relative angle between the c-arm and the breast holder is recorded by a high-resolution angle encoder attached to the C-arm. During a tomosynthesis scan the x-ray tube and detector mounted on a c-arm rotates around the stationary breast continuously over a pre-selected angular range from zero up to 30 degrees in less than 18 seconds. The x-ray tube is pulsed to acquire projections at desired c-arm angles. The x-ray source is located about 55 cm from the rotation axis, and about 66 cm to the detector. The center of the breast is close to the rotation axis of the c-arm.

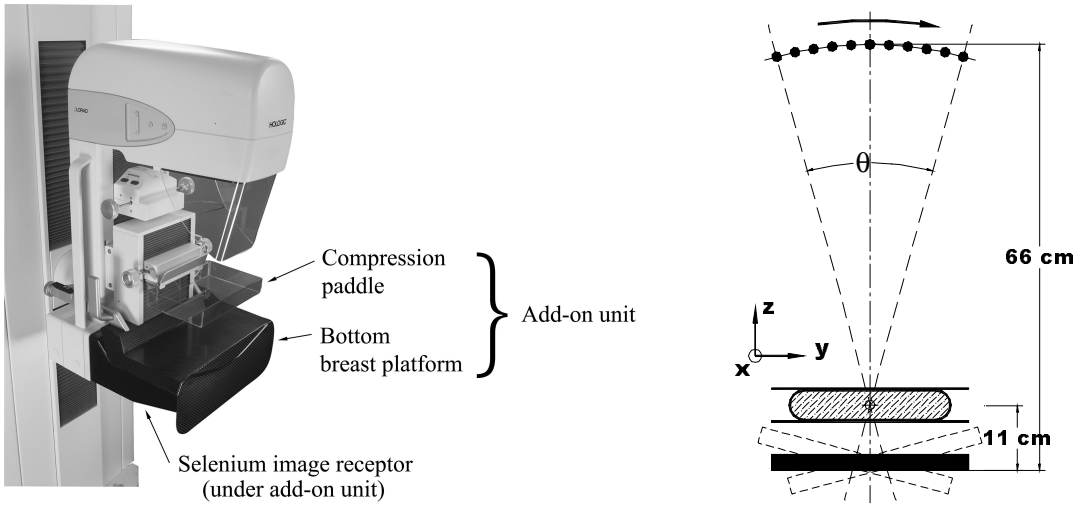

Figure 1: The tomosynthesis prototype uses an add-on unit containing a breast compression paddle and bottom breast platform. The schematic shows it is a moving c-arm design, and it also defines an x-y-z coordinate system for discussions in this paper.

The selenium detector has been previously reported [6]. It is a direct conversion detector with a 70 μm pixel pitch, and an array size of 3328 x 4096, giving a field of view of 24 x 29 cm. During the tomosynthesis acquisition, the detector runs in 2 x 2 pixel binning mode (140 μm pixel pitch), and it takes about 0.6 second to acquire one frame. In the prototype system a total of 11 x-ray exposure images are acquired in 18 seconds during one scan. Although the detector is designed for static radiographic imaging, modifications were made to address tomosynthesis' need of dynamic imaging. Test shows that the ghosting is less than 0.5% frame to frame for the prototype system. A running average of eight frames just before the exposure is used for subtraction of detector's dark current. In tomosynthesis applications, the anti-scattering grid is extracted from the field of view to increase detector signals.

We have tested x-ray sources using either molybdenum (Mo) or a tungsten (W) target. The focal spot size of 0.3 mm is selected during the tomosynthesis scan. The filters in the prototype system are Rh and Al. The high voltage generator has an output range from 20 to 39 kVp, with a maximum tube current of 100 mA between 26 kVp to 34 kVp, and slightly smaller tube current for other kVp values.

Following data acquisition, the eleven acquired images are corrected for offset, bad pixels, and gain variation, and then previewed on the acquisition console before reconstruction. The reconstruction algorithm employed was a modification of filtered backprojection, which allowed for very rapid processing. The images are reconstructed into slices parallel to the breast platform, and typically separated by 1 mm spacing, with a 100 μm in-plane pixel resolution. For a DELL workstation with 1 GB memory, and 3.2GHz Pentium processor, a 50-slice reconstruction takes about one minute.

However, the reconstructed slices are automatically displayed slice by slice as soon as they are available, allowing the operator to start reviewing reconstruction results with very little waiting time. The software allows the slices to be reviewed one by one via mouse wheel control, or dynamically in a cine loop.

RESOLUTION ANALYSIS AND PERFORMANCE

Breast tomosynthesis as a limited angle computed tomography system, has high in-plane resolution in the x-y plane parallel to the breast compression paddle but moderate resolution along the normal z direction. Spatial resolution is one of the critical performance characteristics of a tomosynthesis system and systematic studies were carried out to evaluate it in the prototype system. The method we used is to measure the system MTF using a slanted metal edge [7] at each step from the raw data acquisition to the final reconstruction images, and compare how the shape of MTF curves within the x-y plane have progressed at each step. We also studied the property of "depth of field" of tomosynthesis that relates to the z-resolution of the system.

In the prototype system, the following factors affect the system resolution compared with a conventional Full Field Digital Mammography (FFDM) unit with a similar configuration and a same selenium detector.

1. Detector's pixel binning: The 2x2 binning from a pixel size of 70 μm to 140 μm represents a major source of MTF degradation compared to the conventional digital mammography from Selenia.
2. Blurring from c-arm scanning: For data acquisition scheme with continuous scan and pulsed x-ray shots, the blurring due to the motion of source / detector during the finite x-ray-on time in each of the 11 exposures will smear the object and degrade the MTF.
3. Data interpolation during reconstruction: the bilinear interpolation in the reconstruction process will smear image sharpness.
4. C-arm's geometrical registration: The measurement accuracy of the c-arm position affects the ray tracing during reconstruction. Errors in the geometrical registration will show up as MTF loss.
5. Slice's z-offset from object: When a reconstructed image slice does not intersect the object exactly, the object will show up blurred due to the z-offset.

There are also some additional factors that may likely affect the system MTF performance, e.g., the reconstructed pixel size and the system magnification ratio. Patient motion during a scan will definitely affect the image sharpness in tomosynthesis but it is outside the scope of this paper.

In the following discussions, we will only show MTF curves along the y direction, – which is the direction of the c-arm scanning, – to represent the overall system performance. The MTF curves along the x direction are omitted for brevity's sake, but differences will be mentioned when significant.

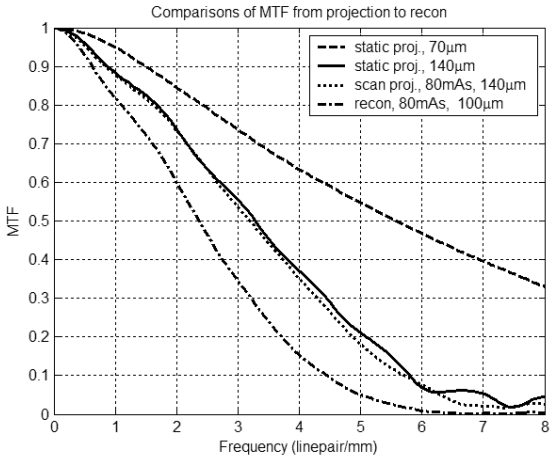

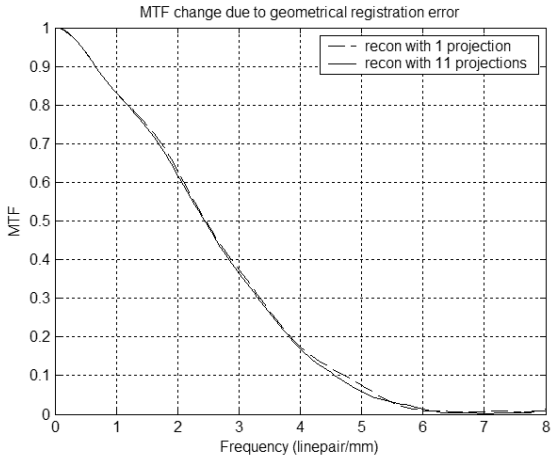

Figure 2 (left): Comparison of MTF from projection to reconstruction along detector's y direction.
Figure 3 (right): MTF reconstructed with either one or all eleven projections at 100 μm pixel size. The difference of the two MTF curves indicates errors from the geometric registration.

In figure 2, we compare several experimentally measured MTF curves of the tomosynthesis system at various stages. The MTF curves here are the MTF response at the system levels, rather than the MTF of the detector itself. The edge phantom was positioned in the center along the chest wall side of the detector, and was 3 cm below the rotation axis. Among the four MTF curves in figure 2, two of them are measured from projection shots when the detector is operated at 70 μm and 140 μm resolution (2×2 binning) modes and the c-arm is stationary, and the third one is from a projection shot of a tomosynthesis scan at 140 μm pixel resolution and 73 ms per x-ray shot, and the fourth one is from a reconstructed image. For ease of discussions through out this paper, here we refer the zero-cutoff frequency of a MTF curve as the "***node frequency*** $\mathbf{f_n}$". Comparing these MTF results, the 2×2 binning makes the detector MTF curve have a node frequency of about 7.5 lp/mm instead of about 14 lp/mm from the no-binned 70 μm pixel sized detector. In addition, since both x-ray focal spot and detector are rotating during the finite duration of x-ray exposure time, c-arm motion degrades the MTF slightly compared to the stationary case. As to the final reconstructed image, the MTF is further degraded since the reconstruction process involves geometry registration, and bilinear interpolation. As we know, the bilinear interpolation has a spatial response function of a triangle shape, and a frequency response of sinc-function squared. Therefore the resolution loss during reconstruction is unavoidable for tomosynthesis, even if the detector runs in the full resolution 70 μm mode. Conventional FFDM will always have a better resolution than the tomosynthesis under similar system configurations.

In figure 3, we check the potential error of the geometrical registration of the system by comparing two MTF curves, one from reconstruction with all eleven projections, and the other from reconstruction with only one of the projections. If there exists significant c-arm geometrical registration error, we would expect to see the backprojected edge image will shift around within the reconstructed slice, and will result in a blurred image compared to an individual projection. The good agreement of two MTF curves indicates our geometrical registration method works very well. Similar agreements of MTF pairs are also found along the x direction, and in a couple of different locations within the volume of a normal sized breast, but these results are not shown here.

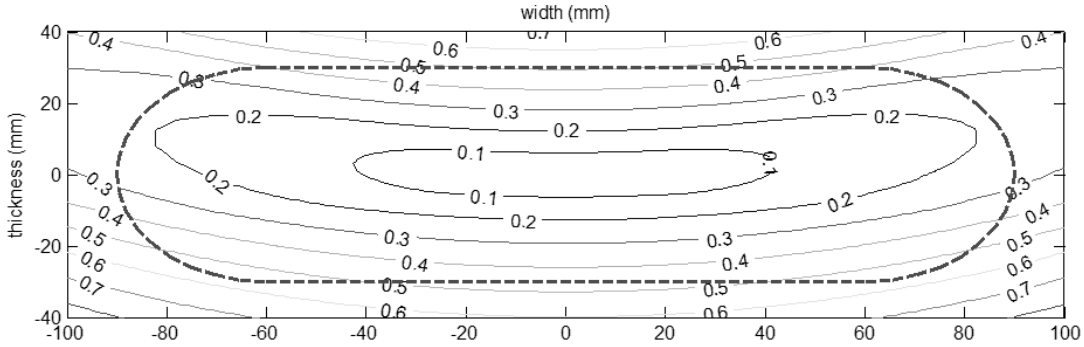

Figure 4: Blurring effect due to moving source and detector simulated with 80 mAs tube loading (100 mA tube current, 800 ms total exposure time for 11 shots). The horizontal axis is width (y) direction, and the vertical is the thickness (z) direction, both in unit of mm. Dashed red region indicates a breast size of 18 cm wide by 6 cm thick, centered with the rotation axis. The blur amount is normalized to one detector pixel size (140 μm) for easy interpretation of the result. As a reference, the source moves about 1.0 mm per exposure of 73 ms (800/11=73) during the scan.

Since scanning of the c-arm during x-ray exposure will blur the image and degrade the system MTF as discussed before, we carried out simulations to determine how short the exposure time should be to give acceptable blurring in the prototype system. Given that the scan takes 18 second over 30 degrees for 11 shots, and generator current is 100 mA, the averaged blurring in a breast reconstructed from 11 individual projection are shown in figure 4, at a typical tube loading of 80 mAs. The blurring amount is normalized to the size of one detector pixel for easy interpretation. The dashed region in the plot represents the cross section of a typical sized breast that is 18 cm wide and 6 cm thick. The results indicate blurring is essentially zero at the rotational center. This initially counterintuitive result is known from conventional linear tomography, where continuous tube and film motion during the x-ray exposure does not result in any blurring at the fulcrum plane. The effective fulcrum in our rotating tomosynthesis c-arm system becomes a point, which is the rotation center of the c-arm. The blurring effect due to focal spot motion increases in general the further one is from this rotation center, and will be worse for larger breasts.

Away from the center, the blur degrades more quickly in the z direction than in the horizontal y direction. For a typical breast of 6 cm thick near the chest wall, we find that the worst blurring amount is about half of the detector pixel size, which is about 70 μm at a tube loading of 80 mAs. The length of blurring amount is proportional to both the tube loading mAs and the breast thickness.

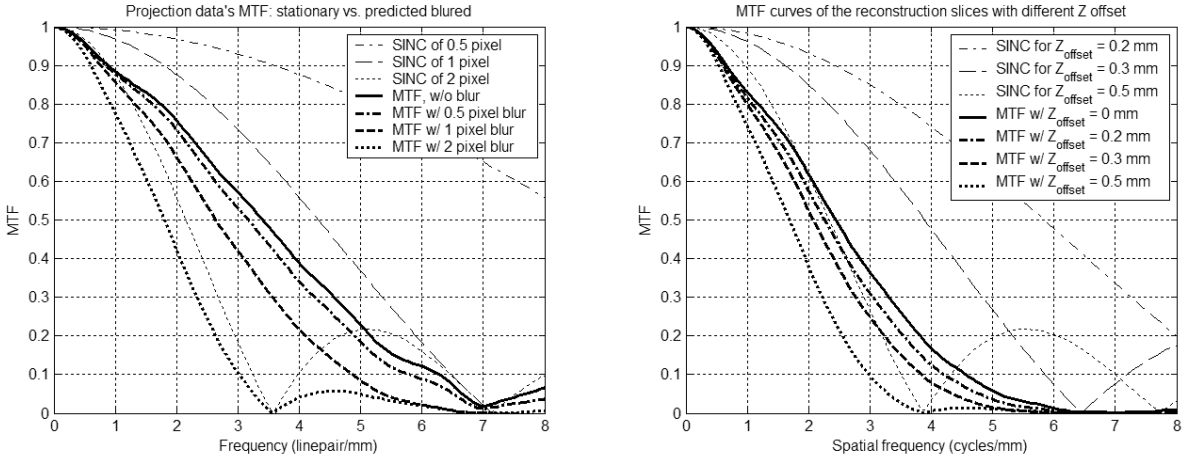

Figure 5 (left): MTF curves with and without c-arm motion, and the corresponding sinc functions of the blurring.
Figure 6 (right): Simulated MTF change versus z-offset, plus the corresponding sinc functions. The node frequency fn of MTF curve without z-offset is found to be 6.5 lp/mm.

The impact of c-arm motion blur to the system MTF at the projection level can be easily seen by multiplying the stationary system MTF with the corresponding sinc function from the motion blur. In figure 5, the MTF of no motion blur and MTF blurred by amount of ½, 1, and 2 times detector pixel size are shown, together with the corresponding sinc functions of each blurring amount. We see that shape of MTF degrades progressively as blurring increases. However, as long as blur is less than a pixel size, the node frequency of the sinc function is larger than that of the MTF curve f_n when there is no motion blur. So the resulted blurred MTF only shows moderate change while keeping the same node frequency f_n. On the other hand, if the blur amount exceeds one pixel, the resulted MTF will have new node frequency smaller than the f_n of the MTF from the stationary c-arm, resulting in a new MTF with a dramatic change of shape and smaller node frequency. Comparing the change of MTF shapes versus different blurring, the node frequency f_n is probably the point that MTF undergoes a qualitative change. Subjectively, we assume that the system could take a blur up to one detector pixel size with less noticeable smearing effect on the image. We did additional simulations to study the appearance of micro-calcifications under different system MTF response curves shown in figure 5, and the results support the above assumption.

Given a certain slice-to-slice step size pre-selected during image reconstruction, a randomly situated small object of interest's z location could miss a slice by up to one half of the slice separation distance. The presence of z-offset away from the object of interest will further blur the object and degrade the effective system MTF since a ***point*** object will become a ***line*** object in the reconstruction slice. This additional blurring process can be simply described by a sinc function in frequency space with the corresponding length of blurring. The figure 6 shows how z-offset affects system MTF. For a small z-offset value, the corresponding sinc-function has a larger node frequency that will only moderately degrade the MTF; however a large z-offset will have a small node frequency less than the node frequency of the MTF. Based on a similar discussion for figure 5, we could take a blurring amount up to the point that the node frequency of the sinc function meets the node frequency f_n of the MTF at focus.

DEPTH OF FIELD IN TOMOSYNTHESIS

Tomosynthesis is like a camera system in that it has a certain depth of field (DOF) with features outside the DOF being out of focus. Conventional radiography and CT systems are at the two extremes with one having infinite and the other

essentially zero DOF, respectively. A clear definition of the DOF is needed for tomosynthesis since it will help to characterize this important tomosynthesis-specific property, and helps to choose a reasonable slice-to-slice separation to avoid missing information during image reconstruction. For a classical camera system (figure 7A), the DOF refers to the range of distance for which the subject is rendered with "acceptable" sharpness [8]. DOF of a camera depends a subjective factor called the "circle of least confusion" (CLC). Extending the idea to linear breast tomosynthesis, the DOF of tomosynthesis can be defined to refer to distance range for which the object can be reconstructed with acceptable sharpness. The equivalent term of CLC of camera system would be the "line of least confusion" (LLC) in tomosynthesis. The physical significance of LLC is that it refers to the effective system resolution within a reconstruction slice for tomosynthesis. From the resolution analysis on z-offset in the previous section, LLC is defined as blurring length at which the node frequency of its sinc function equals to the node frequency f_n of the system MTF for the in-focused slice (see Eq. 1, and figure 6). Following a simple geometry in tomosynthesis, DOF relates to LLC as shown in Eq. 2 and figure 7B. The angle θ is the total angle of the c-arm scan. For example in figure 6, the f_n of the prototype system is about 6.5 lp/mm, θ is 28 degrees, so DOF is found to be about 0.6 mm. The reconstructed slice-to-slice distance should be set to no greater than 0.6 mm to maintain optimal sharpness for the best viewing of micro-calcifications imaged in this geometry. Though our theoretical analysis suggests that a maximum 0.6 mm slice-to-slice separation is needed for ideal micro-calcification visualization, larger masses and lesions show little or no visual difference between adjacent slices 0.6 mm. Very small z step sizes require massive amounts of image data for storage and reviewing. We have found in practice that a display slice separation of 1 mm was a good practical compromise between having a sharp in-focus display of microcalcifications and minimizing the total number of slices. Further work is underway to determine the optimal slice separation needed clinically.

$$LLC = 1/f_n \qquad \text{(Eq. 1)}$$

$$DOF = LLC \Big/ \tan\left(\frac{\theta}{2}\right) \qquad \text{(Eq. 2)}$$

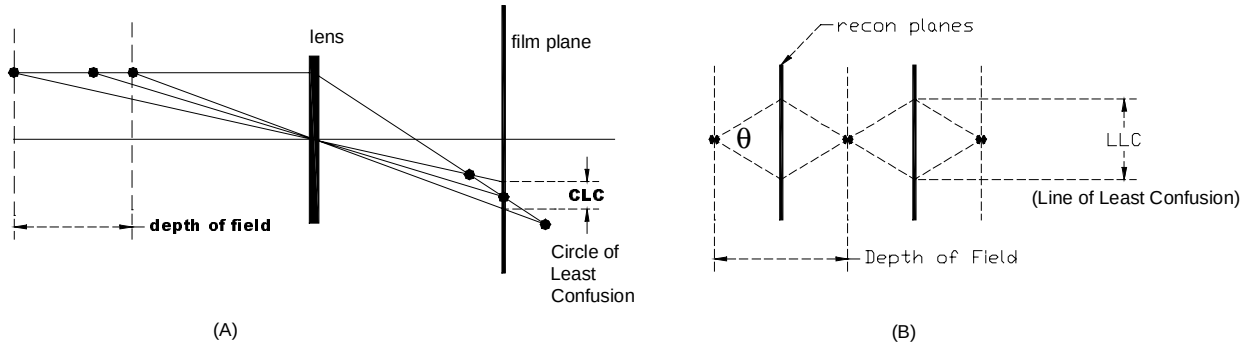

Figure 7: Depth of field in (A) a classical camera system, and in (B) a linear breast tomosynthesis system.

The depth of field depends on two factors (in Eq. 2), the LLC and the scan angle θ.

1. The value of LLC and therefore the node frequency f_n of the MTF of an object at the focused slice, which depends on the overall system MTF performance, e.g., detector's MTF, focal spot size, geometrical registration, blurring due to c-arm motion, reconstructed pixel size and so on. In particular, DOF depends on the detector's MTF and thus the detector pixel size. If the detector pixel size of 70 μm is used in the system, the node frequency of MTF is then, for simplicity of the discussion, just doubled. The reconstruction pixel sizes in the x-y plane and along the z-axis need to be halved in order to keep the full system resolution that the new detector pixel size of 70 μm is providing.
2. The scan angle θ of tomosynthesis system. Given a fixed LLC, the smaller the scan angle θ, the larger the DOF. So for a smaller θ angle scan, one does not need to reconstruct so many slices in the z direction and still

being able to keep acceptable in-slice resolution. This could be advantageous for some tomosynthesis applications.

SIGNAL / NOISE ANALYSIS, SPECTRA OPTIMIZATION

For tomosynthesis, the total dose comparable to the conventional mammogram (1 to 2 ×) is equally divided into 11 shots, and each exposure is essentially a low dose one. Compared with our FFDM product Selenia, the following modifications are applied to the tomosynthesis system to increase signal levels:

1. The detector operates at 2×2 binning mode. This allows fast readout speed, better signal / noise performance, aggressive ghosting suppression between frames.
2. No HTC anti-scattering grid, which increases detector signal.
3. High kVp technique, using W target tube, or Mo tube with Al filter to allow harder x-ray beam.

To optimize x-ray spectra for this system, and to develop operation technique charts, we performed both simulation studies and experiments. A simulation package was developed to calculate mean glandular dose under various test conditions [9]. The package also models the x-ray spectra that match measured HVL values and air exposures. Our system can interchangeably have either a Mo or W target x-ray tube installed, with optimal filters for each tube identified separately. We took empirical approaches to check the signal-to-noise performance and to select proper filters for each tube. The phantoms used for the evaluation studies were the ACR accreditation phantom wax insert, plus the BR 12 breast equivalent phantom. For a given tube target / filter combination under consideration, we measured the phantom with a total of 11 shots similarly to a tomosynthesis acquisition except that the c-arm was set stationary and normal to the phantom. The dose for each thickness was set following what conventional mammograms would deliver at that thickness, but the kVp and mAs are varied to cover a range of both high and low kVp values with practical tube loading mAs. We examined the detector's signal level and contrast to noise ratio (CNR) from both the mass group and micro-calcification groups to identify optimal operation settings. Extensive studies have been carried out to test the two tubes and choices of filter. In figure 8 and 9 we show two representative results of 4.5 cm and 6 cm thick phantoms as examples. They were taken with a W tube, and with the following filters -- 25 μm Rh, 50 μm Rh, 0.4 mm Al, and 0.7 mm Al. The mean glandular dose was set to 200 mrad for the 4.5 cm thick phantom, and 290 mrad for the 6 cm phantom. The CNR of mass is from the first mass group, and CNR of Calcium (Ca) are from the average of the six individual Ca of the first Ca group in the ACR phantom. The CNR results are averaged over eleven tomosynthesis shots to represent the tomosynthesis reconstruction.

In Figure 8, the detector signal, CNR of mass and Ca are plotted either against the kV, or against the mAs to show different perspectives of the data since they are all under a same dose of 200 mrad. In tomosynthesis, we could choose any kVp values allowed by the machine as long as the resulting CNR is optimal. However, we cannot choose very large mAs values since it will result in excessive c-arm motion blur to the image. From our resolution study, the optimal value of mAs is found to be no greater than 80 mAs for acceptable blurring. Looking at the CNR versus kV curves, 50 μm Rh filter seems to be advantageous. However, from CNR versus mAs curves, we find that the 50 μm Rh cannot be selected since it requires very high mAs values to realize the better CNR values. If our system had a 200 mA generator instead of the current 100 mA one, under the same amount of blurring allowance the actual mAs could be pushed as high as 160 mAs. Then the 50 μm Rh filter can be a best choice to give high CNR for both mass and Ca. Unfortunately in the current prototype system, the high voltage generator is not powerful enough to select 50 μm Rh. Between 25 μm Rh and 0.7 mm Al, they both give similar optimal CNR at 80 mAs, but the detector signaler is high for 0.7 mm Al filter than that for the 25 μm Rh filter.

The results in figure 9 are for a 6 cm thick phantom taken under 290-mrad doses, and we see the potential advantage from the 50 μm Rh filter disappears even if large mAs value is used. The 25 μm Rh filter also has lower CNR values compared with Al 0.7 mm filter for both mass and Ca.

We have also carried out similar studies with other phantom thickness, whose results are not shown. From the results of 4.5 cm and 6 cm phantoms, and these other thickness, we determined filters for the W tube – use the 25 μm Rh filter for breast thickness below 4.5 cm, and the 0.7 mm Al filter for thickness greater than or equal to 4.5 cm. The imaging

technique tables are also developed with consideration of blurring requirement, detector signal level, and contrast noise performance. Based on separate spectra optimization studies for a Mo tube (result plots not shown in this paper) filter selections are: 0.4 mm Al filter for breasts equal to or above 4.5 cm thick, and 25 μm Rh filter for breasts below 4.5 cm thick. Comparing Mo and tungsten tubes under a same dose to the breast, the tungsten system gives greater detector signal with less tube-loading mAs, and thus is good for suppressing detector noise and minimizing c-arm motion blurring to the image.

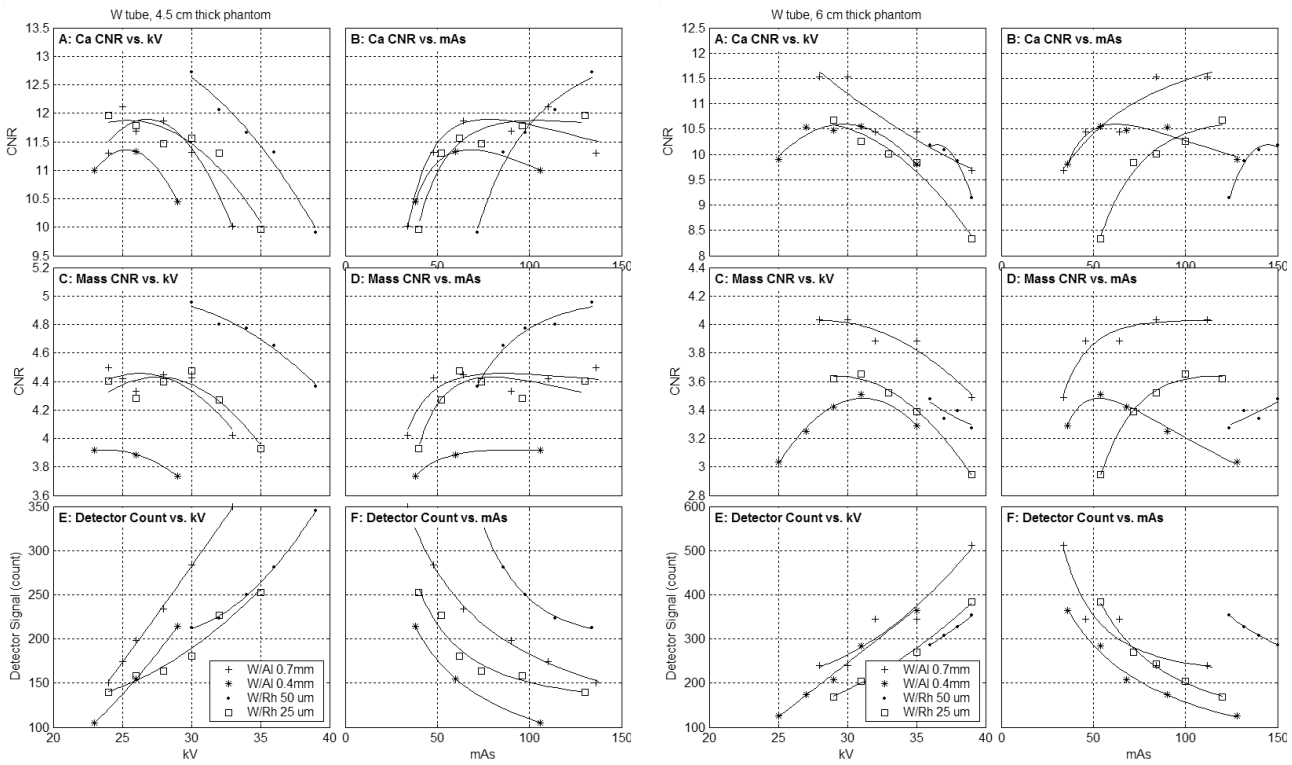

Figure 8 (left): Detector signal and CNR results of 4.5 cm phantoms, doses are equal to 200 mrad for all test points.
Figure 9 (right): Detector signal and CNR of 6 cm phantoms, doses are equal to 290 mrad for all test points.

PERFORMANCE -- PHANTOM AND CLINICAL IMAGES

We have performed both phantom and patient studies to evaluate the performance and image quality of the system. Two cases are shown in this paper, one from a phantom study and the other a patient example.

ACR plus breast phantom

In this study (figure 10), an ACR accreditation phantom wax insert (7mm thick) was positioned on top of a cadaver breast phantom (4.5 mm thick), and they were imaged with both tomosynthesis and conventional mammography with the same dose for comparison. The conventional mammogram was taken with Mo tube, 25 μm Mo filter, 27 kVp, 120 mAs, with the anti-scatter HTC grid. The tomosynthesis scan was taken with W tube, 0.7 mm Al filter, 28 kV, 88 mAs, no HTC grid. The dose is about 230 mrad. The tomosynthesis images are reconstructed at a pixel size of 120 μm in plane, and 0.5 mm slice separation. In the conventional mammogram, we can see the first two groups of micro-Ca easily, and the third group of Ca with some efforts, but no fiber group and no mass group are visible, due to the present of overlapping structure in the background. In the tomosynthesis image, we can see up to the third group of micro-Ca easily, and the fifth group of fiber, and the first group of mass. Tomosynthesis exhibits advantage in showing low contrast features and Ca of a certain size better through the removal of overlapping structure.

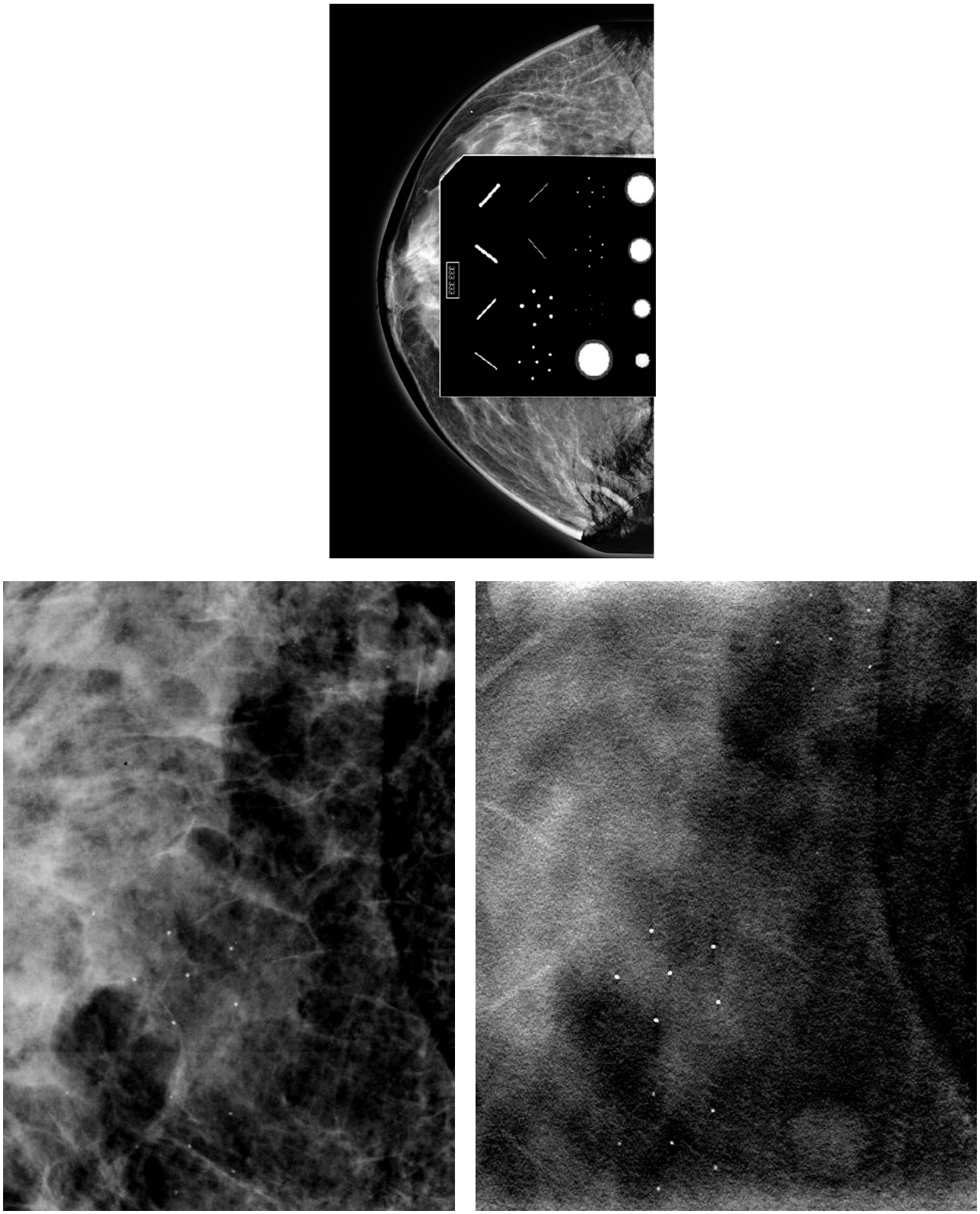

Figure 10: ACR+cadaver phantom: top: full size breast image superimposed with a foreign ACR phantom image; bottom left: ROI with ACR in the mammogram; bottom right: tomosynthesis ROI with ACR.

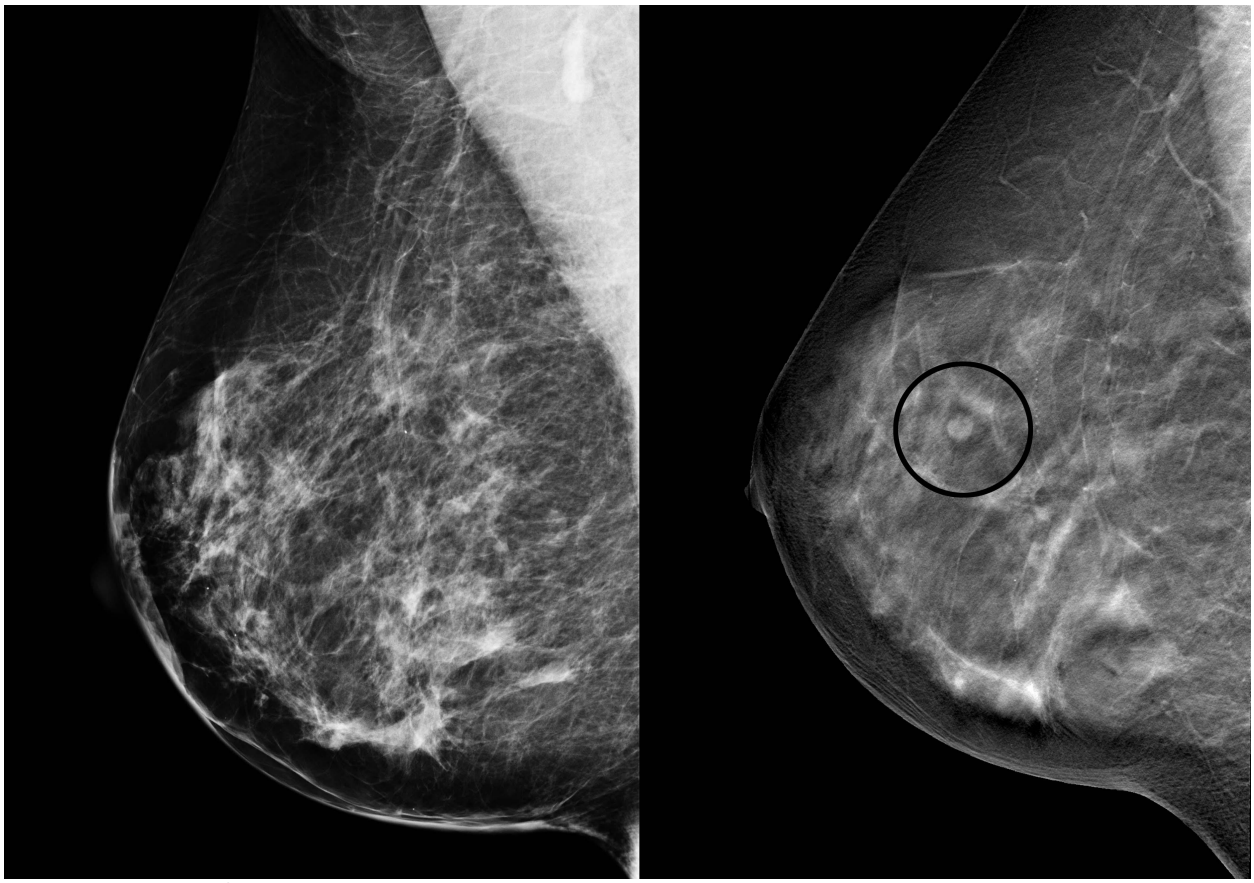

Figure 11: Example of patient image showing tomosynthesis can see a mass better than the mammogram.

Patient study

In figure 11, the image on the left is the conventional Selenia digital mammogram. The image on the right shows the corresponding tomosynthesis image at a slice that shows a lesion, which is occult in the conventional mammogram. It can be seen in the tomosynthesis slice to be a benign fat-containing mass. This lesion was visible in the CC but not the MLO digital mammogram, and represents a false positive mammogram because it went to biopsy and was proven to be benign. The tomosynthesis scan was taken at two times the conventional FFDM dose with a Mo tube and Al filter.

DISCUSSIONS

Resolution analysis shows that the following factors degrade the spatial resolution of our tomosynthesis prototype: 1). detector 2×2 binning; 2). bilinear interpolation during reconstruction; 3). blurring due to c-arm motion; 4). blurring due to the z-offset. Even if the detector is not 2×2 binned, the presence of the other three factors will still degrade a tomosynthesis system's resolution compared to its mammographic counterpart. This finding is applicable to tomosynthesis systems in general. One advantage of selenium direct conversion detectors are their very high resolution. Even with the 2×2-binning mode, the detector's MTF performance is still fairly good. Looking at the MTF response of the detector itself in figure 12, we find that the 2×2 binned mode has MTF performance close to that of indirect conversion detectors with 100 μm pixel size over the clinically relevant spatial frequency range up to 5 lp/mm [10].

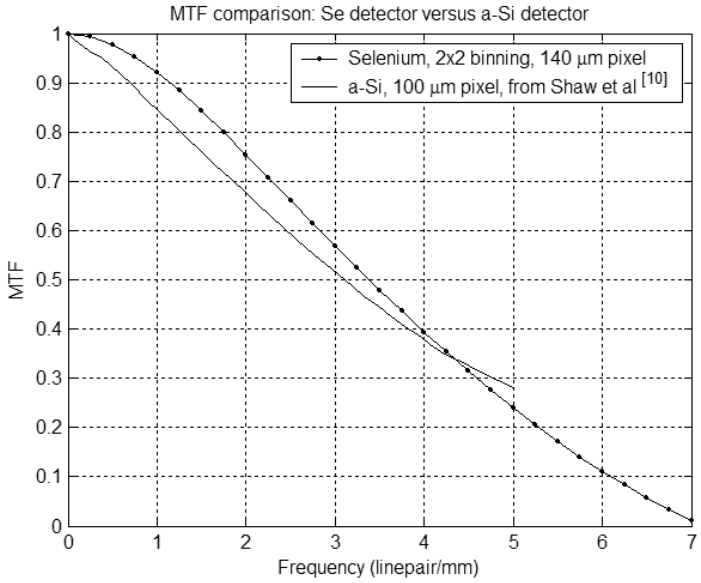

Figure 12: Comparison of MTF curves from selenium direct conversion detector with 2x2 binning (140μm pixel), and CsI indirect conversion detector (100μm pixel) from reference [10]. Selenium based detector has superior MTF generally, even with 2x2 binning mode, the MTF is still comparable to an indirect conversion detector operated with much smaller pixel size.

In the prototype system, operating the detector in 2×2 binning mode offers us the following advantage: 1). Due to the low radiation dose spent on each of the 11 projection shots, the detector binning would help to reduce both electronic and statistical noises. 2). The 140 μm pixel size in this case doubles the DOF of the system compared with that of the 70 um, and the overall reconstruction data size is reduced to 1/8 of that of the 70 um. Given the fact that a typical tomosynthesis reconstructed image set is about 300 Mbytes (for 18 x 24 x 5 cm^3 volume, 120 μm in-plane pixel size and 1mm slice to slice separation), this is very helpful for data processing, storage and reviewing in practice. Initial patient trials are underway to determine if 2×2 binning provides adequate clinical performance.

There are many reports on spectra optimization for mammography systems [11,12]. These results cannot be applied to tomosynthesis directly since the optimal operation setting of tomosynthesis considers not only good signal-to-noise ratio, but also good spatial resolution. Our results indicate that, in general, tomosynthesis will need high kV technique and x-ray beam with higher mean energy than conventional mammography. This finding is in agreement with the trend indicated by the development of cone beam breast CT [13], in which even higher kV and mean beam energy is used to keep the total mean breast dose comparable to the conventional while allowing the increased number of low dose projections needed in CT applications.

Low contrast detectability and system resolution have been two complimentary indexes that characterize the performance of an imaging modality. Comparing radiography versus CT, radiography has superior resolution, and CT system has superior low contrast detectability despite poorer resolution. Tomosynthesis is not intended to compete with conventional mammography in resolution. Instead, the advantage of it is to offer better low contrast detectability through the removal of structure noise. Several studies have shown that in a variety of imaging tasks it is the anatomical structure, rather than the detector's DQE, that limits the performance of radiography [14,15]. For mammography, under the current clinical irradiation dose level, anatomical structure dominates the noise in the image. Further increasing the radiation dose level, or improving the detector noise performance will probably not improve the cancer detection rate by much. Tomosynthesis, as an emerging new technology, fits into the gap between the conventional radiograph and CT by providing 3D structure information with moderately high in-plane resolution, but greatly improved in-slice low contrast detectability. Our image-based evaluations with phantoms and patients show that, by removing the structure noise that presents in the conventional mammogram, tomosynthesis is able to see the feature of interest with better visibility. Additionally, some of the suspicious regions in conventional mammogram are really

due to the overlapping of structures from different slices. Tomosynthesis offers promise to clarify some of these suspicious regions and reduce the false positive rate.

CONCLUSIONS

We have successfully designed and constructed a prototype breast tomosynthesis system using a selenium based direct conversion flat panel detector. Experimental results indicate it works very well as a research system in the hospital. Clinical studies are in progress. Based on the knowledge learned, we are designing a next generation commercial tomosynthesis system with further improved performance.

ACKNOWLEDGEMENTS

We would like to thank the many colleagues at Hologic, and our clinical collaborators whose efforts made this on-going development work possible.

REFERENCE

1. Niklason LT. and et al, Digital tomosynthesis in breast imaging. Radiology. 205(2): 399-406.
2. Wu T. and et al, Tomographic mammography using a limited number of low-dose cone-beam projection images. Med. Phys., 30(3), 365-380.
3. Rafferty EA, and et al, Eliminating the Fake Out: Comparison of Conventional Two View Film Screen Mammography with Full-Field Digital Tomosynthesis in Distinguishing Mammographic Abnormalities from Superimposition of Normal Breast Structures. Radiology 225(P) Supplement 2002: 683.
4. Rafferty EA, and et al, Optimization of Image Acquisition and Display Algorithms to Enhance Visualization of Microcalcifications during Digital Breast Tomosynthesis. Radiology 229(P) Supplement 2003: 423.
5. Lehtimaki M, and et al, Diagnostic clinical benefits of digital spot and digital 3D mammography following analysis of screening findings. Proc. SPIE Vol. 5029, p. 698-706.
6. Yorker JG, and et al, Characterization of a full-field digital mammography detector based on direct x-ray conversion in selenium. Proc. SPIE Vol. 4682, p. 21-29.
7. Samei E and Flynn MJ, A method for measuring the presampled MTF of digital radiographic systems using an edge test device. Med. Phys., 25(1), 102-113.
8. http://www.cs.mtu.edu/~shene/DigiCam/User-Guide/950/depth-of-field.html
9. Boone JM, Glandular Breast Dose for Monoenergetic and High-Energy X-ray Beams: Monte Carlo Assessment1, Radiology 213:23-37.
10. Vedantham S. and et al, Full breast digital mammography with an amorphous silicon-based flat panel detector: Physical characteristics of a clinical prototype, Med. Phys., 27(3), 558-567.
11. Fahrig R., and Yaffe MJ.,Optimization of spectral shape in digital mammography: Dependence on anode material, breast thickness, and lesion type. Med. Phys., 21(9), 1473-1481.
12. Flynn, M., and et al, Optimal radiographic techniques for digital mammograms obtained with an amorphous selenium detector, SPIE 5030, 147-156.
13. Chen B, et al, Cone-beam volume CT breast imaging: feasibility study, Med Phys., 29(5):755-70.
14. Keelan, BW et al, Relative impact of detector noise and anatomical structure on lung nodule detection, SPIE 5372, p230-241.
15. Bochud FO et al, The importance of anatomical noise in mammography, SPIE 3036, p74-80.